A semi-analytical method for oblique gust - cascade interaction

Hongbin Ju[*], Ramani Mani [1]

GE Global Research Center, One Research Circle, Niskayuna, NY, 12309, USA

ARTICLE INFO

ABSTRACT

A semi-analytical method is proposed for calculating the response of a linear cascade with spanwise mean flow subject to oblique gusts. It is developed based on the boundary value problems defined by Lloyd and Peake (AIAA paper 2008–2840). A gust strength parameter is introduced and the correct three-dimensional (3-D) response is obtained. The classic similarity rules are extended; the approach can be used to extend any 2-D methods to account for oblique gusts and 3-D mean flows. It is validated against analytical approximations for single-airfoil and cascade responses. The method is used to investigate the effect of gust angle α_g on the unsteady lift and the sound field. It is found that as α_g increases, the 2-D equivalent response varies slightly. However, the 3-D lift is amplified by factor $1/\cos\alpha_g$, and the spanwise phase variation increases. Cascade effects are also studied. The inter-blade phase angle (IBPA) is important even for very low solidity. As the solidity increases, the chordwise distribution of lift is no longer leading-edge dominant. Cascade effects are small only when the cascade blade count is lower than a limit. A statistics analysis reveals that Mach number is the most important parameter for determining this blade count limit, and frequency is the least important.

© 2018 Elsevier Ltd. All rights reserved.

1. Introduction

The philosophy in turbofan engine designs today is to maximize the bypass ratio (BPR). It benefits both engine efficiency and noise reduction. As BPR increases, jet noise is significantly reduced and fan noise becomes more important. Fan noise tends to overtake jet noise and dominate at all conditions in the next generation of engines.

Fan noise includes tones and broadband noise (BBN). With the development of mitigation technologies in the past few decades, tone noise can now be effectively controlled; BBN is receiving more attention in new engine developments and academic research. There are two types of fan broadband noises: the self-noise and the interaction noise [1]. Self-noise is generated by turbulence in airfoil surface boundary layers scattered at blade trailing edges (TE). Interaction noise is generated by turbulent flows interacting with downstream blade rows. The most important broadband noise source is the interaction between fan wakes and outlet guide vanes (OGV). Depending on the operation conditions, fan self-noise and noise generated by casing boundary layer - fan tip interaction may also be important.

Nomenclature

a_0	sound speed in the mean flow, dimensional, velocity scale
C	airfoil chord length, dimensional, length scale
$\widehat{h}_{mn}^{\pm}(k_1, k_2, k_3)$	chordwise integrated unsteady lift
$\widehat{h}_s^{+}$	$= \sqrt{\sum |\widehat{h}_{mn}^{+}|^2}$ (summation over all the cut-on modes)
K	$= k_1 M_{\xi} / \beta_M^2$
K_s	vortical wavenumber magnitude
k_1, k_2, k_3	vortical wavenumbers in the ξ, η, and z directions respectively
k_d	ω / a_0, acoustic wavenumber
L	unsteady lift due to oblique gust - cascade interaction
l	unsteady lift due to 2-D gust - cascade interaction calculated by LINSUB
M	U_0 / a_0, Mach number
M_{ξ}	$u_{0\xi} / a_0$, Mach number in the ξ direction
m	spinning mode number
N_v	number of the blades
n	radial mode index
p	acoustic pressure
R	radius at which the annular duct is unwrapped
$\overline{R}_r$	rth acoustic pressure at the reference blade leading edge calculated by LINSUB
S	spacing between blades in the linear cascade
$\mathbf{u} = (u_{\xi}, u_{\eta}, u_z)$	unsteady velocity vector & its components
$U_0, \mathbf{u}_0$	mean flow velocity magnitude and vector
w	$\sqrt{\frac{2}{3}\mathrm{TKE}}$, time-averaged upwash velocity
x, y	axial and tangential coordinates in the unwrapped duct coordinate system
z	spanwise coordinate along the leading edge of the reference blade
α_s	gust angle to the ξ-axis
α	wavenumber in the x (axial) direction
β	wavenumber in the y direction
β_M	$= \sqrt{1 - M_{\xi}^2}$, compressibility parameter
Γ_j	parameters defined in Eqs.(20) & (28)
η	chord-normal coordinate on the reference blade
θ	stagger angle of the linear cascade
Λ	turbulence integral length scale
λ	$\omega / u_{0\xi}$, reduced frequency
ξ	chord-wise coordinate on the reference blade, normal to the blade leading edge
ρ_0	density of the mean flow, dimensional, density scale
σ	βS, inter-blade phase angle (IBPA)
φ	acoustic velocity potential
ψ	mean flow angle to the ξ-axis
ω	circular frequency
ω_e	$= \omega - k_3 u_{0z} = k_{s1} u_{0\xi}$, effective frequency

Subscripts

0	mean flow
r	acoustic wave index
s	source (vortical component)
a	acoustic component

Superscript

*	complex conjugate
Caret ""	Fourier components
Over bar '-'	variables in two dimensions
$\pm$	downstream (+) and upstream (-)
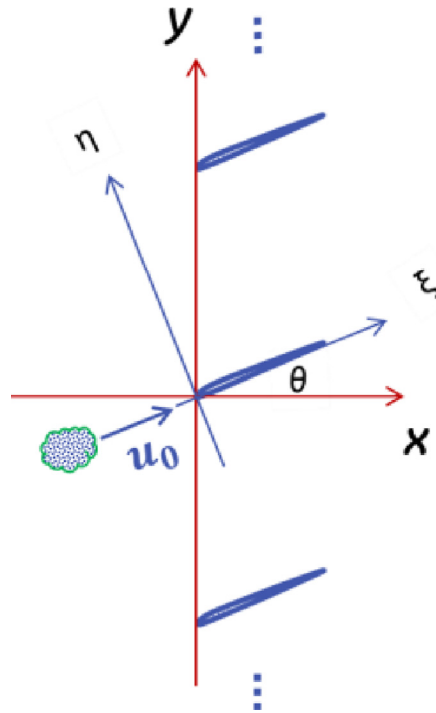
Fig. 1. Gust - cascade interaction. (Span-wise coordinate z is normal to the paper.)

Vorticity waves in the upstream turbulent flow convect through the cascade (Fig. 1), inducing the normal component of the vortical velocity on the blade surfaces. To satisfy the impermeable boundary condition at the blade surfaces, the normal component of the acoustic velocity and the sound wave are generated. The normal vortical velocity is the ultimate driver of the interaction noise. The cascade has two effects. One is to scatter an incident vorticity wave into other vorticity waves [2]. The other effect is the acoustic interaction between the blades and the occurrence of cascade resonances under some conditions. In a ducted engine, the duct has a significant effect on sound propagation. It cuts off acoustic waves with high wavenumbers, only letting a limited number of modes to propagate (cut-on).

Modeling noise generation and propagation involves two steps: the cascade harmonic analysis and the broadband modeling. In the first step, a method is developed to calculate the response from a cascade subject to a harmonic vorticity wave. For an unloaded flat-plate cascade in a uniform flow shown in Fig. 1, a harmonic wave with frozen vorticity has this form:

$$\Gamma e^{i(k_1\xi+k_2\eta+k_3z-\omega t)}, \ \omega = k_1 u_{0\xi} + k_3 u_{0z}. \tag{1}$$

ξ is the coordinate on the reference blade, normal to the blade leading edge. z is the spanwise coordinate along the leading edge. η is the coordinate normal to both ξ and z. k_1, k_3, and k_2 are wavenumbers in these three directions. Γ represents the strength of the vorticity wave. The source of the broadband noise is the random turbulence in the flow. Since turbulence is composed of correlated/uncorrelated harmonic waves in a wide spectral range, the second step, broadband modeling, is needed to compute the sound power.

Cascade harmonic analyses are fundamental for broadband noise predictions. Hundreds of gust - cascade responses are calculated to predict the sound power at each frequency. Quick turnaround computation is critical for predicting a spectrum. Analytical or semi-analytical methods are preferred. Over the years, several analytical solutions have been proposed. High- and low-frequency approximations for 3-D gust - single airfoil interactions were developed by Adamczyk using the Wiener-Hopf technique [3,4], and by Amiet using the Schwarzschild's theorem [5]. The blade tip end effect was accounted for in the Amiet's theory by Roger et al. using a composite two-dimensional Schwarzschild's technique [6]. The 3-D gust - linear cascade response using the Wiener-Hopf technique was proposed by Glegg [7] and Posson *et.al.* [8]. A high frequency model for 3-D gust - annular cascade interaction was developed by Envia [9]. Some semi-analytical models have also been developed, such as the 2-D bound vorticity model LINSUB by Smith [2], the lift model for 3-D gust - annular cascade by Namba [10], and the lift model for 2-D gust - linear cascade by Ventres *et.al.* [11], etc. Based on these harmonic analyses, several broadband models and codes have been developed. Based on Glegg's analytical harmonic analysis [7], Hanson developed the BBCascade code [12]. Morin extended it to 3-D using the strip theory and developed the BFaNS code [1]. Nallasamy and Envia [13] developed

the RSI code based on Ventres *et.al.*'s semi-analytical harmonic analysis [11]. The RSI code was explored and validated by Grace [25]. Posson and Moreau proposed a model based on their analytical cascade response function [26]. Cheong et al. developed a broadband model based on LINSUB [14].

Cascade harmonic analyses for 3-D gust - annular cascade, such as Namba's model [10], account for realistic geometries and mean flows. However, broadband models based on these analyses may be very complex, with little flexibility to adapt to even slightly different geometries or flows. They are not necessarily the best choices in applications [11]. On the other hand, methods based on 2-D theories are easier to develop and are more flexible in applications. For example, LINSUB was modified for perforated cascades by Reba and Morin [15].

In 2-D methods, assumptions must be made for responses with $k_3 \neq 0$. If turbulence lengthscales are small and duct modal shapes change little within the integration range, in the region away from the duct walls the 2-D gust ($k_3 = 0$) makes most contribution to the noise. Responses from oblique gusts cancel each other and can be simply disregarded [13]. This leads to under-predictions of sound power level (PWL) when compared with methods that include oblique gust effects [16]. On the other hand, equal responses from all k_3 are assumed in some methods; and sound power is usually over-predicted [14]. Obviously, it is necessary to study oblique gust effects and account for them in the response.

Two major effects of an oblique gust are illustrated in Fig. 2. The spanwise phase gradient ($ik_3 e^{ik_3 z}$) is first introduced. This increases the source cancellation and more sound waves are cut off, both reducing the sound power in the far field. On the other hand, the phase gradient and the source cancellation in the chordwise direction are reduced. The reduced frequency decreases as the gust tilts and the cascade response becomes stronger according to the Sear's function. For a long blade (aspect ratio $\gg 1$), the benefit from the spanwise source cancellation is larger than the chordwise noise penalty; therefore the tone noise in the far field is reduced. This is the major mechanism of the tone noise reduction in swept cascade configurations. Sweep of blades also introduces secondary effects, such as introducing the spanwise mean flow, reducing effective inflow velocity, and reducing the inter-blade phase angle, etc [7].

Theories fully accounting for 3-D gusts include: Filotas [18] and Mugridge [19] for incompressible flows, Adamcyzk [3] and Amiet [5] for isolated airfoils in compressible flows, Namba [10] for annular cascades, Martinez and Widnall [20] for rectangular wings with finite span, Goldstein [17] and Atassi and Hamad [21] for rectilinear cascade with endwalls, Glegg [7] and Posson et al. [8] for linear cascades, *etc*. Recently there are attempts to extend 2-D methods to account for oblique gusts. For example, the integral equation in LINSUB was modified by Reba and Morin to calculate responses from 3-D gusts interacting with a perforated cascade [15]. Similarity rules and 2-D equivalence theories were also developed, in which only the inputs to a 2-D method need to be modified. Graham [28] and Adamcyzk [4] reveal that the response from an isolated airfoil only depends on two parameters. Similar analyses apply for cascades, except that parameters related to the cascade geometry are also involved. Atasii and Hamad [21] developed the similarity rules for cascades in 2-D flows. Lloyd and Peake [22] further considered 3-D mean flows. They found that all the five inputs to LINSUB need to be modified and the equivalent 2-D lift was directly used in the 3-D response. However, the similarity rules in Eq. (80) and the acoustic pressure in Eq. (85) in Ref. [22] are not consistent with Eqs. (7), (26) and (27) in Ref. [21] when the span-wise mean velocity is zero.

The 2-D equivalence method in Ref. [22] is revisited in this paper. Similar boundary value problems are defined; but a different solving procedure is proposed. It is found that, in addition to the five inputs to LINSUB, the upwash velocity also needs to be modified. The 3-D lift is not equal to the equivalent 2-D lift. The method is validated against analytical solutions by Adamcyzk for isolated airfoils [4] and by Posson et al. for linear cascades [8]. Since there is no need to modify original 2-D methods, this approach is very useful for extending any existing 2-D models to account for 3-D gusts and 3-D mean flows.

The rest of the paper is arranged as follows. The boundary value problem (BVP) for the oblique gust - cascade interaction and the BVP for the 2-D gust - cascade interaction are defined respectively in sections 2 and 3. The equivalent 2-D problem is discussed in Section 4. The 3-D response is derived in Section 5. The major results are the similarity rules in Eq. (32), the lift
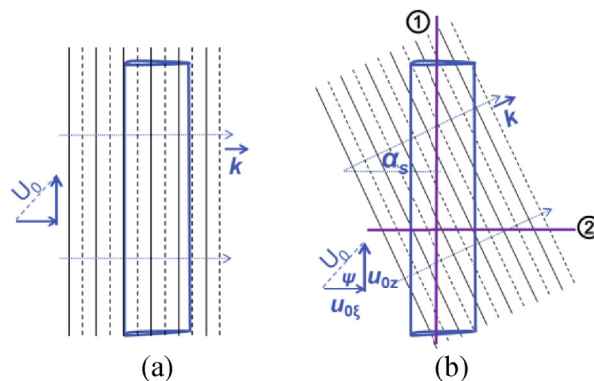
Fig. 2. Effects of an oblique gust interacting with a linear cascade. (a) 2-D gust ($k_3 = 0$); (b) 3-D (oblique) gust ($k_3 \neq 0$): ① higher spanwise phase gradient → more source cancellation & cutoff modes for tones, ② less chordwise phase gradient → lower reduced frequency → higher response.

distribution on blades in Eq. (34), and the acoustic solution in Eq. (37). The method is validated against analytical solutions in Section 6. Effects of oblique gusts and cascades are discussed in Section 7. Concluding remarks are made in Section 8.

2. 3-D vorticity wave - cascade interaction

2.1. The linear Euler equations

Two coordinate systems shown in Fig. 1 are used in the analysis. Cascade coordinates (ξ, η, z) are convenient for describing the turbulent flow (the acoustic source) since the upwash velocity is in the η direction. Duct coordinates (x, y, z) are suitable for describing sound propagation in the duct. In the cascade coordinate system, the linearized Euler equations for an adiabatic process are:

$$\frac{Dp}{Dt} + \frac{\partial u_\xi}{\partial \xi} + \frac{\partial u_\eta}{\partial \eta} + \frac{\partial u_z}{\partial z} = 0, \tag{2}$$

$$\frac{Du_\xi}{Dt} + \frac{\partial p}{\partial \xi} = 0, \tag{3}$$

$$\frac{Du_\eta}{Dt} + \frac{\partial p}{\partial \eta} = 0, \tag{4}$$

$$\frac{Du_z}{Dt} + \frac{\partial p}{\partial z} = 0, \tag{5}$$

$$\frac{D\rho}{Dt} = \frac{Dp}{Dt}, \tag{6}$$

where

$$\frac{D}{Dt} = \frac{\partial}{\partial t} + u_{0\xi}\frac{\partial}{\partial \xi} + u_{0z}\frac{\partial}{\partial z}.$$

Variables with subscript '0' are mean flow quantities. Others such as p are perturbations. All variables are non-dimensional. The scales for these variables are: length: chord C, velocity: sound speed a_0, time: C/a_0, density: ρ_0, and pressure: $\rho_0 a_0^2$.

It has been shown that the blade geometry (thickness and camber) and the flow angle of attack mainly affect the steady force [17,22]. Their impact on unsteady loading is in higher orders. A recent numerical study confirms that the blade thickness has effects only at high frequencies [27]. An unloaded flat-plate cascade is considered in this paper. The mean flow is uniform and parallel to the cascade plates.

This form of Fourier components with time factor $e^{-i\omega t}$ is adopted in the paper:

$$p(\xi, \eta, z, t) = \text{Re}\left\{\widehat{p}(k_1, k_2, k_3, \omega)e^{i(k_1\xi + k_2\eta + k_3 z - \omega t)}\right\}, \text{ etc.} \tag{7}$$

The analysis applies for positive or negative ω. If time factor $e^{i\omega t}$ were used, ω in all the formulas should be replaced by $-\omega$. Substituting Eq. (7) in Euler Eqs. (2)–(6), one finds three families of linear waves: vorticity waves, acoustic waves, and entropy waves [2]. Wavenumbers k_1, k_2 and k_3 satisfy three dispersion relations. Vorticity waves and entropy waves have frozen patterns. They are determined by upstream boundary conditions. If there are no entropy waves in the upstream flow, the solution to Eq. (6) is simply:

$$\rho = p.$$

Similar equations can also be established in the duct coordinate system for

$$p(x, y, z, t) = \text{Re}\left\{\widehat{p}(\alpha, \beta, k_3, \omega)e^{i(\alpha x + \beta y + k_3 z - \omega t)}\right\}, \text{ etc.}$$

α and β are wavenumbers in the x and y directions respectively. The relations between the two coordinate systems are:

$$\begin{aligned}
&\xi = x\cos\theta + y\sin\theta, \ \eta = -x\sin\theta + y\cos\theta, \\
&\alpha = k_1\cos\theta - k_2\sin\theta, \ \beta = k_1\sin\theta + k_2\cos\theta, \\
&\alpha x + \beta y = k_1\xi + k_2\eta.
\end{aligned} \tag{8}$$

θ is the stagger angle. The last equation indicates that the phase of a plane wave remains unchanged in the two coordinate systems.

2.2. Vorticity waves as the source of gust - cascade interaction

We consider upstream vorticity waves as the source of the gust - cascade interaction. A vorticity wave carries no fluctuating pressure ($\widehat{p}_s = 0$); associated with it is only fluctuating velocity $\widehat{\mathbf{u}}_s$. Subscript 's' denotes the source. The following relations must hold to satisfy Euler Eqs. (2)–(6):

$$\omega_e \equiv \omega - k_3 u_{0z} = k_{s1} u_{0\xi}, \tag{9}$$

$$k_{s1} \widehat{u}_{s\xi} + k_{s2} \widehat{u}_{s\eta} + k_3 \widehat{u}_{sz} = 0. \tag{10}$$

Only one Fourier component is to be considered in the z direction. Since $e^{ik_3 z}$ is a common factor for all the waves, k_3 is used instead of k_{s3}. To define a unique vorticity wave, five of the seven variables, such as $\widehat{u}_{s\eta}$, $\widehat{u}_{sz}$, k_1, k_3, and ω, need to be prescribed. Amplitudes $\widehat{u}_{s\eta}$ and $\widehat{u}_{sz}$ are usually determined from the turbulence kinetic energy (TKE), turbulence integral length scale $\varLambda$, and a turbulence spectrum model such as the Liepmann spectrum, the Karman spectrum, or the Gaussian spectrum. For the other three parameters, it is convenient to prescribe $\beta_s (= k_{s1} \sin\theta + k_{s2} \cos\theta)$, k_3, and ω for engine noise studies.

The upwash velocity at the cascade blades induced by the vorticity wave is:

$$\widehat{u}_{s\eta} e^{i(k_{s1}\xi + k_{s2}\eta + k_3 z - \omega t)} = \widehat{u}_{s\eta} e^{i\left[\omega_e \xi / u_{0\xi} + (\beta_s - \omega_e \sin\theta / u_{0\xi})jS + k_3 z - \omega t\right]}, \tag{11}$$

for $jS \sin\theta \leq \xi \leq jS \sin\theta + 1$, $\eta = jS \cos\theta = 2\pi jR \cos\theta / N_v$, $j = 0,1,\ldots, N_v\text{-}1$. N_v, S and R are respectively the blade count, the spacing between two blades, and the radius at which the annular cascade is unwrapped. ω_e is the effective frequency defined in Eq. (9). $j = 0$ represents the reference blade; $j = 1$ is the blade above the reference blade, *etc.*

2.3. The boundary value problem defined in acoustic velocity potential

Define the acoustic velocity potential φ:

$$\mathbf{u}_a = \nabla\varphi, \tag{12}$$

$$p = -\frac{D\varphi}{Dt}. \tag{13}$$

Assume this form of acoustic waves:

$$\varphi(\xi, \eta, z, t) = \text{Re}\{\breve{\varphi}(\xi, \eta, k_3, \omega) e^{i(k_3 z - \omega t)}\}, ,$$

$$p(\xi, \eta, z, t) = \text{Re}\{\breve{p}(\xi, \eta, k_3, \omega) e^{i(k_3 z - \omega t)}\}..$$

Substituting them in Eq. (2)–(5) and (12)–(13) yields

$$\left(-i\omega_e + u_{0\xi}\frac{\partial}{\partial\xi}\right)^2 \breve{\varphi} - \left(\frac{\partial^2}{\partial\xi^2} + \frac{\partial^2}{\partial\eta^2} - k_3^2\right)\breve{\varphi} = 0, \tag{14}$$

$$\breve{p} = \left(i\omega_e - u_{0\xi}\frac{\partial}{\partial\xi}\right)\breve{\varphi}. \tag{15}$$

Apply the *Prandtl-Glauert* transformation:

$$\xi = \xi, \ \eta' = \beta_M \eta, \ \tilde{\varphi}(\xi, \eta', k_3, \omega) = \breve{\varphi}(\xi, \eta, k_3, \omega) e^{iKM_\xi \xi}, \tag{16}$$

$$K = \omega_e \big/ \beta_M^2 = k_{s1} M_\xi \big/ \beta_M^2, \ M_\xi = u_{0\xi}, \ \beta_M = \sqrt{1 - M_\xi^2}.$$

Then acoustic Eq. (14) can be written in terms of $\tilde{\varphi}$ as:

$$\left(\frac{\partial^2}{\partial\xi^2}+\frac{\partial^2}{\partial\eta'^2}+K^2-\frac{k_3^2}{\beta_M^2}\right)\widetilde{\varphi}=0.\tag{17}$$

Formally it is the acoustic wave equation in a stationary medium. The boundary condition at the blades, Eq. (11), is recast as:

$$u_{a\eta}=-u_{s\eta}=-\widehat{u}_{s\eta}\mathrm{e}^{\mathrm{i}\left[\omega_e\xi/u_{0\xi}+(\beta_s-\omega_e\,\sin\,\theta/u_{0\xi})jS+k_3z-\omega t\right]},\,i.e.,$$

$$\frac{\partial\widetilde{\varphi}}{\partial\eta'}=-\frac{\widehat{u}_{s\eta}}{\beta_M}\mathrm{e}^{\mathrm{i}\left[K\xi/u_{0\xi}+(\beta_s-\omega_e\,\sin\,\theta/u_{0\xi})jS\right]},\tag{18}$$

for $jS\sin\theta\le\xi\le jS\sin\theta+1$, $\eta'=j\beta_M S\cos\theta$, $j=0,1,\ldots,N_v$-1.

The Kutta condition requires the continuous pressure at the blade trailing edges and in the wakes:

$$\Delta\breve{p}=0.$$

Applying (15) on both sides of the wake, the Kutta condition is satisfied if

$$\left(\mathrm{i}\omega_e-u_{0\xi}\frac{\partial}{\partial\xi}\right)\Delta\left[\widetilde{\varphi}(\xi,\eta',k_3,\omega)\mathrm{e}^{-\mathrm{i}KM_\xi\xi}\right]=0,$$

$$i.e.,\left(\mathrm{i}-\frac{M_\xi}{K}\frac{\partial}{\partial\xi}\right)\Delta\widetilde{\varphi}=0,\tag{19}$$

for $\xi\ge jS\sin\theta+1$, $\eta'=j\beta_M S\cos\theta$, $j=0,1,\ldots,N_v$-1.

Eqs. 17–19 form a complete boundary value problem for $\widetilde{\varphi}$. Its solution is determined by six parameters:

$$\Gamma_1=\sqrt{K^2-(k_3/\beta_M)^2},\ \Gamma_2=K\big/M_\xi,\ \Gamma_3=\left(\beta_s-\omega_e\sin\theta\big/u_{0\xi}\right)S$$

$$\Gamma_4=S\sin\theta,\ \Gamma_5=\beta_M S\cos\theta,\ \Gamma_6=\widehat{u}_{s\eta}/\beta_M.\tag{20}$$

For the gust - isolated airfoil response, the solution only depends on three parameters: cut-off parameter Γ_1, frequency parameter Γ_2, and gust strength parameter Γ_6. The other three parameters, Γ_3, Γ_4 and Γ_5, are related to the cascade geometry. It is noted that gust strength parameter Γ_6 was not considered by Lloyd & Peake [22].

Once $\widetilde{\varphi}$, or $\mathrm{i}\Gamma_2\widetilde{\varphi}-\partial\widetilde{\varphi}/\partial\xi$, is known, the acoustic pressure is determined from Eq. (15), or:

$$\breve{p}=u_{0\xi}\mathrm{e}^{-\mathrm{i}KM_\xi\xi}(\mathrm{i}\Gamma_2\widetilde{\varphi}-\partial\widetilde{\varphi}/\partial\xi).\tag{21}$$

3. 2-D vorticity wave - cascade interaction

Based on Eq. (17), it is possible to define an equivalent frequency to account for the k_3 effect. However, k_3 also appears in the source [Eq. (18)] and in the Kutta condition [Eq. (19)]. All the variables, not only the frequency, need to be accounted for in the 2-D equivalence problem.

Both the gust and the mean flow are assumed to be two dimensional. Variables in two dimensions are denoted by overbar '-'. The 2-D cascade coordinates are related to the duct coordinates by

$$\xi=\overline{x}\cos\overline{\theta}+\overline{y}\sin\overline{\theta},\ \overline{\eta}=-\overline{x}\sin\overline{\theta}+\overline{y}\cos\overline{\theta}.$$

Define acoustic velocity potential $\overline{\varphi}$:

$$\overline{\mathbf{u}}_a=\nabla\overline{\varphi},\ \overline{p}=-\frac{\overline{\mathrm{D}}_\xi\overline{\varphi}}{\mathrm{D}t},\ \frac{\overline{\mathrm{D}}_\xi}{\mathrm{D}t}=\frac{\partial}{\partial t}+\overline{u}_{0\xi}\frac{\partial}{\partial\xi}.\tag{22}$$

Assume the Fourier components

$$\overline{\varphi}(\xi, \overline{\eta}, t) = \mathrm{Re}\left\{\breve{\widetilde{\varphi}}(\xi, \overline{\eta}, \overline{\omega})\mathrm{e}^{-\mathrm{i}\overline{\omega}t)}\right\}, \ \ \overline{p}(\xi, \overline{\eta}, t) = \mathrm{Re}\left\{\breve{\widetilde{p}}(\xi, \overline{\eta}, \overline{\omega})\mathrm{e}^{-\mathrm{i}\overline{\omega}t)}\right\}. \tag{23}$$

Applying the *Prandtl-Glauert* Transformation:

$$\xi = \xi, \ \ \eta' = \overline{\beta}_M \overline{\eta}, \ \ \widetilde{\varphi}(\xi, \eta', \omega) = \breve{\widetilde{\varphi}}(\xi, \overline{\eta}, \overline{\omega})\mathrm{e}^{\mathrm{i}\overline{KM}_\xi \overline{\xi}}, \tag{24}$$

$$\overline{K} = \overline{\omega}\big/ \overline{\beta}_M^2, \ \ \overline{\beta}_M = \sqrt{1 - \overline{M}^2}, \ \ \overline{M} = \overline{u}_{0\xi},$$

the acoustic equation in terms of $\widetilde{\varphi}$ is:

$$\left(\frac{\partial^2}{\partial \xi^2} + \frac{\partial^2}{\partial \eta'^2} + \Gamma_1^2\right)\widetilde{\varphi} = 0. \tag{25}$$

Γ_1 is to be defined later in Eq. (28). It will be shown that the variables such as ξ, η', $\tilde{\varphi}$, and Γ_1 in the 3-D BVP are the same as in the equivalent 2-D BVP. Therefore over bar '-' is omitted on these variables.

The boundary condition at the blade surfaces is:

$$\frac{\partial \widetilde{\varphi}}{\partial \eta'} = -\Gamma_6 \mathrm{e}^{\mathrm{i}(\Gamma_2 \xi + \Gamma_3 j)}, \tag{26}$$

for $j\Gamma_4 \le \xi \le j\Gamma_4 + 1$, $\eta' = \Gamma_5 j$, $j = 0,1,\ldots, N_v$-1.

The Kutta condition at the blade trailing edges and in the wakes is:

$$\left(\mathrm{i} - \frac{1}{\Gamma_2}\frac{\partial}{\partial \xi}\right)\Delta \widetilde{\varphi} = 0, \tag{27}$$

for $\xi > j\Gamma_4 + 1$, $\eta' = \Gamma_5 j$, $j = 0,1,\ldots, N_v$-1.

Eq. (25)–(27) form a BVP for two dimensional gusts interacting with the linear cascade. $\tilde{\varphi}$ is uniquely determined by these six parameters:

$$\Gamma_1 = \overline{K}, \ \Gamma_2 = \overline{K}\big/\overline{M}_\xi, \ \Gamma_3 = \left(\overline{\beta}_s - \overline{\omega}\sin\overline{\theta}\big/\overline{u}_{0\xi}\right)\overline{S}, \ \Gamma_4 = \overline{S}\sin\overline{\theta}, \ \Gamma_5 = \overline{\beta}_M \overline{S}\cos\overline{\theta},$$
$$\Gamma_6 = \hat{\overline{u}}_{s\eta}\big/\overline{\beta}_M. \tag{28}$$

Acoustic pressure is computed by [ref. Eq. (21)]:

$$\breve{\widetilde{p}} = \overline{u}_{0\xi}\mathrm{e}^{-\mathrm{i}\overline{KM}_\xi \xi}(\mathrm{i}\Gamma_2 \widetilde{\varphi} - \partial\widetilde{\varphi}/\partial\xi). \tag{29}$$

4. The equivalent 2-D problem

BVPs for acoustic potential $\widetilde{\varphi}(\xi, \eta', \omega)$ in 3-D [Eq. (17)–(19)] and in 2-D [Eq. (25)–(27)] have exactly the same form. If the six parameters in Eq. (20) match those in Eq. (28), the two problems have the same solutions in the transformed coordinate system (ξ, η') shown in Fig. 3(a).

The cut-on condition for acoustic waves in the 3-D case is:

$$\frac{\left[\beta\left(1 - M_\xi^2\right) + M_y \omega_e\right]^2}{1 - M_x^2} + k_3^2\left(1 - M_\xi^2\right) < \omega_e^2.$$

For cut-on modes in a subsonic flow,

$$k_3^2 \le \omega_e^2\big/\beta_M^2. \tag{30}$$

We can define an equivalent 2-D problem by matching the parameters in Eqs. (20) and (28):
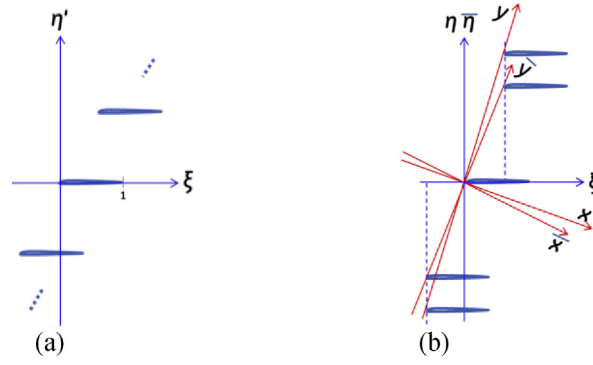
Fig. 3. (a) The 2-D BVP and the 3-D BVP have the same geometry and solutions in the transformed coordinate system (ξ, η'). (b) In the physical coordinate systems the two problems have different geometries and mean flows.

$$
\begin{aligned}
&\Gamma_1 = \overline{K} = \pm\sqrt{K^2 - (k_3/\beta_M)^2}, \; (+ \text{ if } \omega_e \geq 0, \; - \text{ if } \omega_e < 0), \\
&\Gamma_2 = \overline{K}\big/\overline{M}_\xi = K\big/M_\xi, \\
&\Gamma_3 = \overline{\beta}_s\overline{S} - \overline{\omega}\overline{S}\sin\overline{\theta}\big/\overline{u}_{0\xi} = \beta_s S - \omega_e S \sin\theta\big/u_{0\xi}, \\
&\Gamma_4 = \overline{S}\sin\overline{\theta} = S\sin\theta, \; \Gamma_5 = \overline{\beta}_M\overline{S}\cos\overline{\theta} = \beta_M S \cos\theta, \; \Gamma_6 = \overline{\hat{u}}_{s\eta}\big/\overline{\beta}_M = \hat{u}_{s\eta}/\beta_M.
\end{aligned}
\tag{31}
$$

From these equations we can determine the six 2-D variables. It is noted that the geometry, the mean flow and the gust are all changed in the physical coordinate systems as shown in Fig. 3(b).

5. The 3-D gust - cascade response

5.1. Solving the 2-D equivalence problem

The three steps to calculate the oblique gust - cascade response are: (1) solve the 2-D Euler equations for acoustic pressure $\breve{p}$; (2) compute $i\Gamma_2\tilde{\varphi} - \partial\tilde{\varphi}/\partial\xi$ from Eq. (29); and (3) calculate the 3-D response from Eq. (21).

Here LINSUB [2] is employed to solve the 2-D equations. The five inputs to LINSUB can be obtained from Eq. (31):

$$
\begin{aligned}
&\text{Mach number: } \overline{M} = \overline{u}_{0\xi} = \Gamma_1/\Gamma_2 = u_{0\xi}\sqrt{1 - (\beta_M k_3/\omega_e)^2}, \\
&\text{Stagger angle: } \overline{\theta} = \tan^{-1}\left[(\tan\theta)\overline{\beta}_M\big/\beta_M\right], \\
&\text{Inverse solidity: } \overline{S} = S\sqrt{\sin^2\theta + \cos^2\theta\left(\beta_M\big/\overline{\beta}_M\right)^2}, \\
&\text{Reduced frequency: } \overline{\lambda} \equiv \overline{\omega}\big/\overline{u}_{0\xi} = \Gamma_2\overline{\beta}_M^2 = \left(\overline{\beta}_M\big/\beta_M\right)^2\lambda_e, \; \lambda_e = \omega_e\big/u_{0\xi} = \lambda - k_3 u_{0z}\big/u_{0\xi}, \\
&\text{Inter} - \text{blade phase angle: } \overline{\sigma} = \sigma + S\sin\theta\left[\left(\overline{\beta}_M\big/\beta_M\right)^2 - 1\right]\lambda_e, \; \sigma = \beta_s S, \; \overline{\sigma} = \overline{\beta}_s\overline{S}.
\end{aligned}
\tag{32}
$$

The physical explanation of these equivalent 2-D parameters is as follows. According to the transformations in Eqs. (16) and (24), lengths in the ξ direction, such as chord C, remain unchanged. Lengths in the perpendicular direction (η') are different. For example, the height between blades in the 2-D equivalence problem is $\overline{H} = H\beta_M/\overline{\beta}_M$, as shown in Fig. 3(b). Therefore the 2-D equivalent stagger angle satisfies $\tan\overline{\theta} = \beta_M \tan\theta/\overline{\beta}_M$. It also explains the inverse solidity since $\overline{S} = \overline{H}/\cos\overline{\theta}$, $S = H/\cos\theta$, $\overline{S}/S = \beta_M\cos\theta/(\overline{\beta}_M\cos\overline{\theta}) = \sin\theta/\sin\overline{\theta}$. It is noted that responses for k_3 and $-k_3$ are equal if $u_{0z} = 0$. This is not true if $u_{0z} \neq 0$.

For isolated-airfoils, $\overline{M}$ and $\overline{\lambda}$ are the only 2-D equivalent parameters needed. They are consistent with Adamczyk's cutoff parameter γ and frequency parameter β defined in Eqs. (3) and (7) in Ref. [4]. If there is no spanwise mean flow ($u_{0z} = 0$), the two parameters reduce to $\overline{M} = M_\xi\sqrt{1 - (1/M_\xi^2 - 1)(k_3/k_1)^2}$ and $\overline{\lambda} = k_1(1 + k_3^2/k_1^2)$, consistent with Graham's M_∞ and k_∞ defined in Eq. (13) in Ref. [28]. For cascade responses, the five equivalent parameters reduce to those defined by Atassi and Hamad in Eq. (26) in Ref. [21] for $u_{0z} = 0$. Compared with the similarity rules defined in Ref. [22], the Mach number and the

reduced frequency we obtained are different from Eqs. (80) and (81) in Ref. [22]. The other three parameters are the same as in Eq. (82)—(84) in Ref. [22].

5.2. The lift

From Eq. (29), the lift on the reference blade ($j = 0$) in the 2-D equivalence problem is:

$$\breve{\overline{L}}(\xi) = \Delta \breve{\overline{p}}(\xi, \overline{\eta} = 0, \overline{\omega}) \equiv \breve{\overline{p}}\left(\xi, \overline{\eta} = 0^-, \overline{\omega}\right) - \breve{\overline{p}}\left(\xi, \overline{\eta} = 0^+, \overline{\omega}\right) = \overline{u}_{0\xi} e^{-i\overline{KM}_\xi \xi} \Delta(i\Gamma_2 \widetilde{\varphi} - \partial\widetilde{\varphi}/\partial\xi).$$

Applying Eqs. (21) and (29), we obtain the lift on the reference blade for oblique gusts:

$$
\begin{aligned}
\breve{L}(\xi) &= \Delta \breve{p}(\xi, \eta = 0, k_3, \omega) = u_{0\xi} e^{-iKM_\xi \xi} \Delta(i\Gamma_2 \widetilde{\varphi} - \partial\widetilde{\varphi}/\partial\xi) \\
&= \left(u_{0\xi} \big/ \overline{u}_{0\xi}\right) \breve{\overline{L}}(\xi) e^{i\left(1 - \overline{\beta}_M^2 \big/ \beta_M^2\right)\omega_e \xi / u_{0\xi}}.
\end{aligned}
\tag{33}
$$

With the inputs from Eq. (32), LINSUB computes $l^*(\xi)$, the lift normalized by $\overline{\rho}_0 \overline{u}_{0\xi}^2$ for gust strength $\overline{\widehat{u}}_{s\eta}^* = \overline{u}_{0\xi}$ and time factor $e^{i\overline{\omega} t}$. (Superscript '*' denotes the complex conjugate.) Then the lift in the 2-D equivalence problem is,

$$\overline{L}(\xi) = \overline{\rho}_0 \overline{u}_{0\xi} \overline{\widehat{u}}_{s\eta} l(\xi).$$

The lift due to the oblique gust - cascade interaction is

$$\breve{L}(\xi) = \rho_0 u_{0\xi} \widehat{u}_{s\eta} \left(\overline{\beta}_M \big/ \beta_M\right) l(\xi) e^{i\left(1 - \overline{\beta}_M^2 \big/ \beta_M^2\right)\omega_e \xi / u_{0\xi}}.
\tag{34}$$

This result is different from Eq. (85) in Ref. [22] in which the factor $\overline{\beta}_M/\beta_M$ is missing. This factor results from the gust strength equivalence parameter introduced in Eqs. (20), (28) and (31). For isolated-airfoils with no spanwise mean flow,

$$\overline{\beta}_M \big/ \beta_M = \sqrt{1 + (k_3/k_1)^2}, \quad \breve{L}(\xi) = \rho_0 u_{0\xi} \widehat{u}_{s\eta} l(\xi) \sqrt{1 + (k_3/k_1)^2} e^{-ik_3^2 \xi / k_1},$$

which is consistent with Graham's similarity rule Eq. (14) in Ref. [28]. For cascades, Eq. (34) reduces to Eq. (27) in Ref. [21] if $u_{0z} = 0$.

5.3. Acoustic waves

The output of the rth acoustic wave from LINSUB, $\overline{R}_r^*$, is the sound pressure normalized by $\overline{\rho}_0 \overline{u}_{0\xi}^2$ at the leading edge $\overline{x}_{LE}$ for gust amplitude $\overline{\widehat{u}}_{s\eta}^* = \overline{u}_{0\xi}$. Therefore, the acoustic pressure in time domain for gust $\overline{\widehat{u}}_{s\eta}$ is

$$\mathrm{Re}\left[\overline{R}_r^* \overline{\rho}_0 \overline{u}_{0\xi} \overline{\widehat{u}}_{s\eta}^* e^{i\left[\overline{\alpha}_r^\pm (\overline{x} - \overline{x}_{LE}) + \overline{\beta}_r \overline{y} + \overline{\omega} t\right]}\right],
\tag{35}$$

where

$$
\begin{aligned}
\overline{\omega} &= \overline{u}_{0\xi}\left(\overline{\beta}_M \big/ \beta_M\right)^2 \omega_e \big/ u_{0\xi}, \quad \overline{\beta}_r = \overline{\beta}_s - 2\pi r \big/ \overline{S} \\
\overline{\alpha}_r^\pm &= \left[\overline{u}_{0x}\left(-\overline{\omega} + \overline{\beta}_r \overline{u}_{0y}\right) \pm \sqrt{\left(\overline{\omega} - \overline{\beta}_r \overline{u}_{0y}\right)^2 - \overline{\beta}_r^2 \left(1 - \overline{u}_{0x}^2\right)}\right] \Bigg/ \left(1 - \overline{u}_{0x}^2\right).
\end{aligned}
$$

For time factor $e^{-i\overline{\omega} t}$, the 2-D equivalent sound pressure is

$$\breve{\overline{p}}_r = \overline{R}_r \overline{\rho}_0 \overline{u}_{0\xi} \widehat{\overline{u}}_{s\eta} e^{i\left[\left(\overline{\alpha}_r^\pm \cos\overline{\theta} + \overline{\beta}_r \sin\overline{\theta}\right)\xi - \left(\overline{\alpha}_r^\pm \sin\overline{\theta} - \overline{\beta}_r \cos\overline{\theta}\right)\eta' \big/ \overline{\beta}_M\right]}.$$

Substituting this into Eqs. (29) and (21), we obtain the rth acoustic pressure for oblique gusts:

$$\begin{aligned}\breve{p}_r^{\pm} &= u_{0\xi}e^{-i\left(KM_\xi - \overline{KM}_\xi\right)\xi}\breve{\overline{p}}_r^{\pm}\Big/\overline{u}_{0\xi} \\ &= \overline{R}_r\overline{\rho}_0 u_{0\xi}\hat{u}_{s\eta}\left(\overline{\beta}_M\Big/\beta_M\right)e^{i\left(1-\overline{\beta}_M^2\Big/\beta_M^2\right)\omega_e\xi/u_{0\xi}}e^{i\left[\left(\overline{\alpha}_r^{\pm}\cos\overline{\theta}+\overline{\beta}_r\,\sin\theta\right)\xi-\left(\overline{\alpha}_r^{\pm}\,\sin\overline{\theta}-\overline{\beta}_r\,\cos\overline{\theta}\right)\eta\beta_M\Big/\overline{\beta}_M\right]}\end{aligned} \tag{36}$$

It can be recast in the duct coordinate system as:

$$\breve{p}_r^{\pm} = \overline{R}_r\overline{\rho}_0 u_{0\xi}\hat{u}_{s\eta}\left(\overline{\beta}_M\Big/\beta_M\right)e^{i\left(\alpha_r^{\pm}x+\beta_r y\right)}, \tag{37}$$

where

$$\beta_r = \overline{\beta}_r\,\sin\theta/\sin\overline{\theta} + \left(1-\overline{\beta}_M^2\Big/\beta_M^2\right)\omega_e\,\sin\theta\Big/u_{0\xi} = \beta_s - 2\pi r/S,$$

$$\begin{aligned}\alpha_r^{\pm} &= \overline{\alpha}_r^{\pm}\cos\overline{\theta}\Big/\cos\theta + \overline{\beta}_r\,\sin\theta\,\cos\overline{\theta}\left(\overline{\beta}_M\Big/\beta_M - \beta_M\Big/\overline{\beta}_M\right) + \left(1-\overline{\beta}_M^2\Big/\beta_M^2\right)k_{s1}\,\cos\theta \\ &= \left\{u_{0x}\left(-\omega+\beta_r u_{0y}+k_3 u_{0z}\right)\pm\left[\left(\omega-\beta_r u_{0y}-k_3 u_{0z}\right)^2 - \left(\beta_r^2+k_3^2\right)\left(1-u_{0x}^2\right)\right]^{1/2}\right\}\Big/\left(1-u_{0x}^2\right).\end{aligned} \tag{38}$$

β_r and $\alpha_r^{\pm}$ are consistent with the 3-D acoustic dispersion relation. The proof of Eq. (38) is given in the Appendix.

The 2-D equivalent responses (lift and acoustic waves) for inter-blade phase angles $\overline{\sigma}+2\pi n$ are the same for any integer n. According to Eq. (32), 3-D responses for $\sigma+2\pi n$ are also the same for any n.

6. Validation

The 2-D equivalence method is first validated on an isolated airfoil configuration. The mean flow and the oblique gust as in Fig. 2 are:

$$\begin{aligned}&u_{0\xi} = U_0\cos\psi, u_{0z} = U_0\sin\psi; \\ &k_1 = K_s\cos\alpha_s,\ k_3 = K_s\sin\alpha_s,\ k_2 = (\sigma/S - k_1\,\sin\theta)/\cos\theta, \\ &\omega = k_1 u_{0\xi} + k_3 u_{0z} = K_s U_0\cos(\psi-\alpha_s).\end{aligned} \tag{39}$$

ψ and α_s are respectively the angles of the mean flow and the gust to the ξ-axis. Only two equivalent parameters in Eq. (32) are required: Mach number $\overline{M}$ and reduced frequency $\overline{\lambda}$. Amiet's high frequency approximation [5] is applied to calculate the 2-D equivalent lift $l(\xi)$, which is substituted into Eq. (34) to obtain the 3-D lift $\breve{L}(\xi)$. $\breve{L}(\xi)$ is compared in Fig. 4 with the analytical approximation [4]. The two results are identical.

The 2-D equivalence method combined with LINSUB is validated on a cascade configuration defined in Ref. [8], Table 3. The gust oblique angle is 26.6°. The predicted unsteady lift is compared in Fig. 5 with the analytical solution from Ref. [8]. Both the real and the imaginary parts match well.
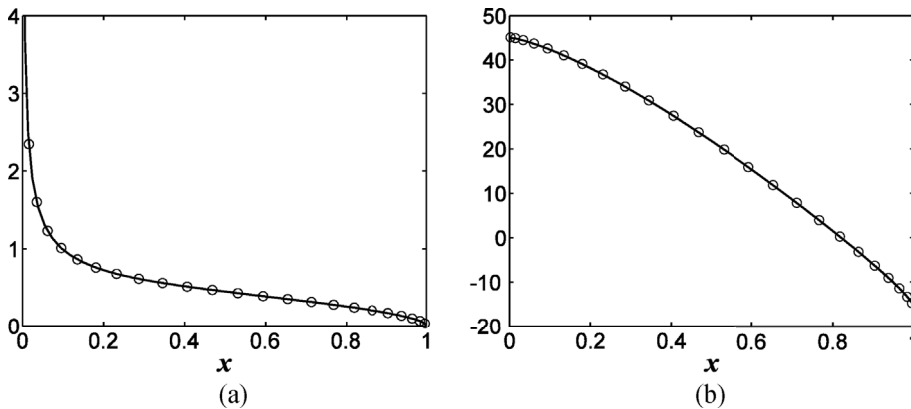
Fig. 4. Normalized lift $\breve{L}(\xi)/(\rho_0 U_0\hat{u}_{s\eta})$ from oblique gust - isolated airfoil interaction at high frequency: (a) magnitude, (b) phase in degree. $M = 0.41$, $K_s = 11.56$, $\psi = 30°$, $\alpha_s = 20°$; 2-D equivalent parameters: $\overline{M} = 0.1$, $\overline{\lambda} = 12.3$. Solid line: 2-D equivalence + Amiet's 2-D gust high frequency approximation [5], symbols: Adamczyk's 3-D gust high frequency approximation [4].
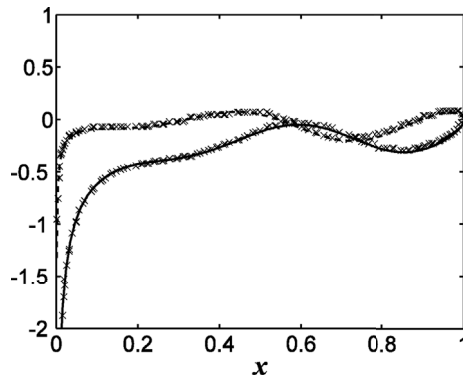
Fig. 5. Unsteady lift $\breve{L}(\xi)$ normalized by $\rho_0 U_0 w_0$ (w_0: incident upwash amplitude at mid-chord). The cascade geometry and the gust parameters defined in Table 3 of [8] are used: $S = 1$, $\theta = 30^0$, $M = 0.5$, $\psi = 0^0$ (no sweep), $k_1 = 20$, $k_2 = 4$, $k_3 = 10$. 2-D equivalent parameters: $\overline{S} = 0.92$, $\overline{\theta} = 32.8^0$, $\overline{M} = 0.25$, $\overline{\lambda} = 25$, $\overline{\sigma} = 15.96$. Solid line: real part of normalized $\breve{L}(\xi)$ from 2-D equivalence + LINSUB, dashed line: imaginary part; symbols: analytical solution from Fig. 5(b) in Ref. [8].

7. Effects of the gust oblique angle and the cascade on lift distribution

7.1. Effects of the gust oblique angle

According to Eqs. (32) and (39),

$$\overline{\lambda} = K_s / \cos\alpha_s, \ \overline{\beta}_M \Big/ \beta_M = 1/\cos\alpha_s. \tag{40}$$

If K_s is held constant, 2-D equivalent reduced frequency $\overline{\lambda}$ increases with gust angle α_s; therefore 2-D lift $l(\xi)$ in Eq. (34) reduces. However, the far-field acoustic wave may still be stronger due to smaller chord-wise phase gradient and less acoustic source cancellation. $\overline{\beta}_M / \beta_M$ in Eq. (34) increases to maximum $1/\beta_M$ for cut-on modes [ref. Eq. (30)]. With the combination of these effects, it is difficult to tell how the 3-D lift $\breve{L}(\xi)$ and the acoustic wave strength vary with the gust angle.

Fig. 6 compares lift $\breve{L}(\xi)$ from gust – isolated airfoil interactions at a high frequency for two gust angles. As α_s increases, the lift magnitude varies very little near the leading edges and the trailing edges. It increases in the mid-chord region between 40% and 70% of the chord. The phase gradient decreases. A similar trend is shown in Fig. 7(a) for the gust - cascade interaction with $\sigma = 0$, except that the phase difference is more substantial. At low frequencies, the effect of the gust angle is smaller, as shown in Fig. 8. The lift is more leading-edge dominant at low frequencies compared to high frequencies. The phase gradient is almost zero in the high lift region from the leading edge to the mid-chord.

(a)   (b)
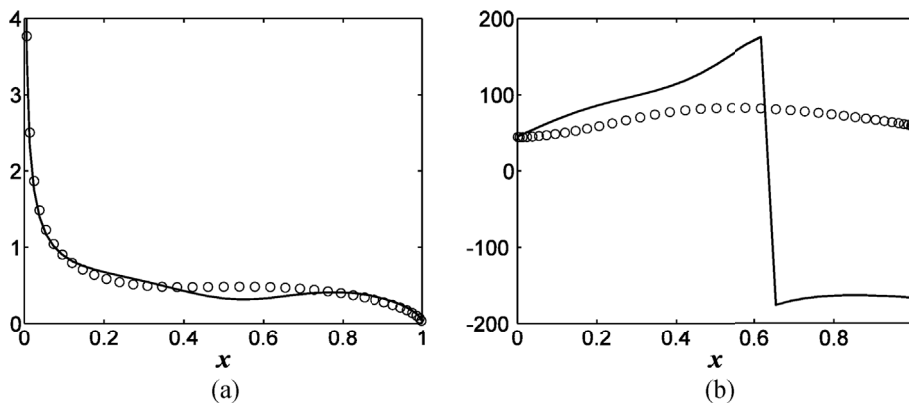
Fig. 6. Lift $\breve{L}(\xi)$ from gust - airfoil interaction at a high frequency using Adamczyk's high frequency approximation [4]: (a) magnitude, (b) phase in degree. $M = 0.41$, $K_s = 11.56$, $\psi = 0^0$. Solid line: $\alpha_s = 0^0$ (2-D equivalent parameters: $\overline{M} = 0.41$, $\overline{\lambda} = 11.56$), symbols: $\alpha_s = 20^0$ (2-D equivalent parameters: $\overline{M} = 0.24$, $\overline{\lambda} = 12.3$).
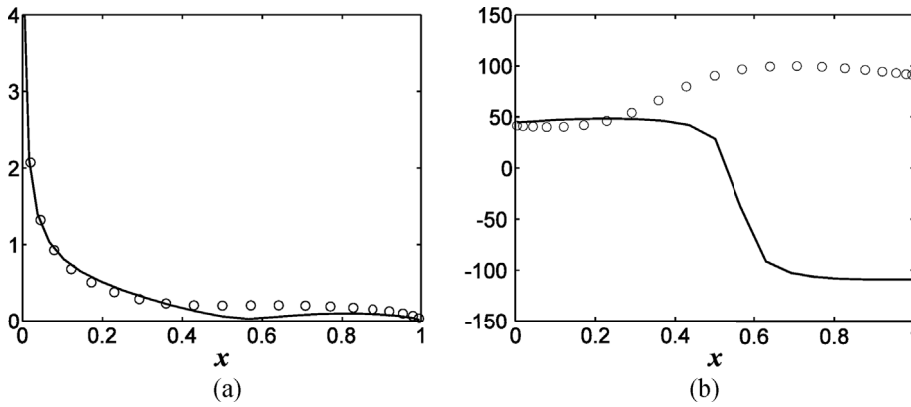
Fig. 7. Lift $\breve{L}(\xi)$ from gust - cascade interaction at a high frequency using 2-D equivalence + LINSUB: (a) magnitude, (b) phase in degree. Solidity: 1.7, $\theta = 10.29^0$, $\sigma = 0$, $M = 0.41$, $K_s = 11.56$, $\psi = 30^0$. Solid line: $\alpha_s = 0^0$ (2-D equivalent parameters: $\overline{S} = 0.59$, $\overline{\theta} = 10.29^0$, $\overline{M} = 0.36$, $\overline{\lambda} = 11.56$, $\overline{\sigma} = 0$), symbols: $\alpha_s = 20^0$ (2-D equivalent parameters: $\overline{S} = 0.55$, $\overline{\theta} = 10.93^0$, $\overline{M} = 0.1$, $\overline{\lambda} = 12.3$, $\overline{\sigma} = 0.15$).
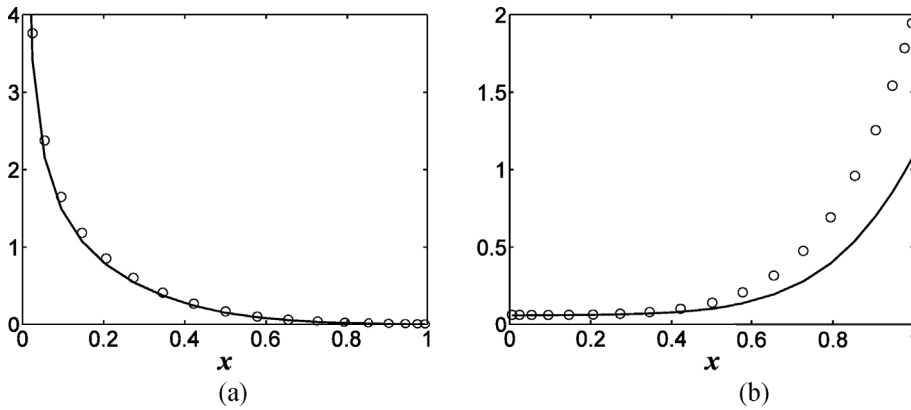
Fig. 8. Lift $\breve{L}(\xi)$ from gust - cascade interaction at a low frequency using 2-D equivalence + LINSUB: (a) magnitude, (b) phase in degree. Solidity: 1.7, $\theta = 10.29^0$, $\sigma = 0$, $M = 0.41$, $K_s = 0.0072$, $\psi = 30^0$. Solid line: $\alpha_s = 0^0$ (2-D equivalent parameters: $\overline{S} = 0.59$, $\overline{\theta} = 10.29^0$, $\overline{M} = 0.36$, $\overline{\lambda} = 0.0072$, $\overline{\sigma} = 0$). symbols: $\alpha_s = 20^0$ (2-D equivalent parameters: $\overline{S} = 0.55$, $\overline{\theta} = 10.93^0$, $\overline{M} = 0.1$, $\overline{\lambda} = 0.0077$, $\overline{\sigma} = 0.0000942$).

Study shows that the effect of the oblique angle on the magnitude of the 2-D equivalent lift $l(\xi)$ is small. Its impact on the phase gradient is larger especially at high frequencies. However, in the high lift region, the phase gradient varies little with the gust angle. Therefore, it is reasonable to use the 2-D gust response $l(\xi)$ for all k_3 in Eq. (34). The major effects of an oblique gust are the spanwise phase variation as in $e^{ik_3 z}$ and the magnitude factor $\overline{\beta}_M/\beta_M$ in Eqs. (34) and (36).

Similar conclusions can be made if the frequency is kept constant as α_s varies.

7.2. 2 Effects of the cascade

Cascade effects are studied by comparing gust - cascade responses with gust - airfoil responses. Two major controlling parameters are IBPA and solidity. For a low-solidity cascade, Fig. 9 shows the effect of IBPA on both the magnitude and the phase of the lift. The leading edge dominance of the lift is no longer applicable for $\sigma = -1.98$. The lift has a node and the phase changes the sign at 13% of the chord.

The effect of solidity is studied for different frequencies with $\sigma = 0$. At high frequencies, as the solidity increases, both the magnitude and the phase are affected, as shown in Fig. 10. At a very high frequency shown in Fig. 11, the lift is no longer leading-edge dominant. The effect of the solidity on the lift magnitude is significant even at low frequencies, as shown in Fig. 12.

7.3. Vane count limit for small cascade effects

Cascade effects are important in the full frequency range if the cascade solidity or the vane count is large. They are accounted for in the 2-D equivalence method combined with the LINSUB. However, this method requires intensive
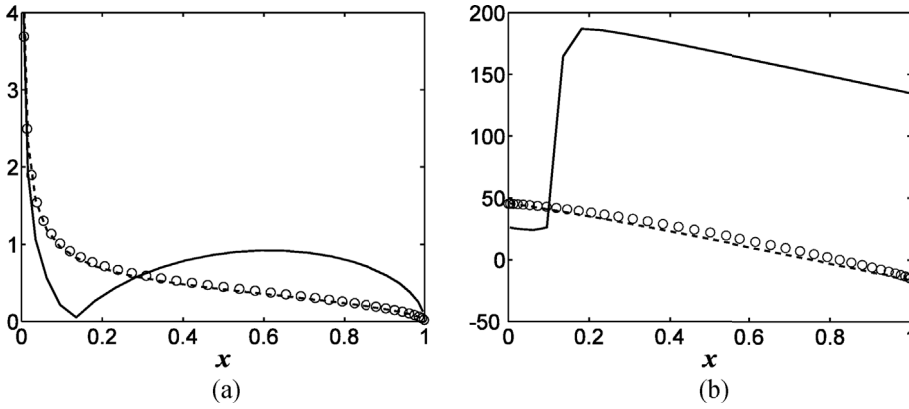
Fig. 9. Lift $\breve{L}(\xi)$ from gust - low-solidity cascade interaction at a high frequency: (a) magnitude, (b) phase in degree. Solidity: 0.0951, $\theta = 10.29^0$, $M = 0.41$, $K_s = 11.56$, $\psi = 30^0$, $\alpha_s = 20^0$. 2-D equivalent parameters: $\overline{S} = 9.9$, $\overline{\theta} = 10.93^0$, $\overline{M} = 0.1$, $\overline{\lambda} = 12.3$. Symbols: single-airfoil approximation [4], dashed line: 2-D equivalence + LINSUB, $\sigma = 3.32$, $\overline{\sigma} = 2.7$; solid line: $\sigma = -1.98$, $\overline{\sigma} = 0.72$.
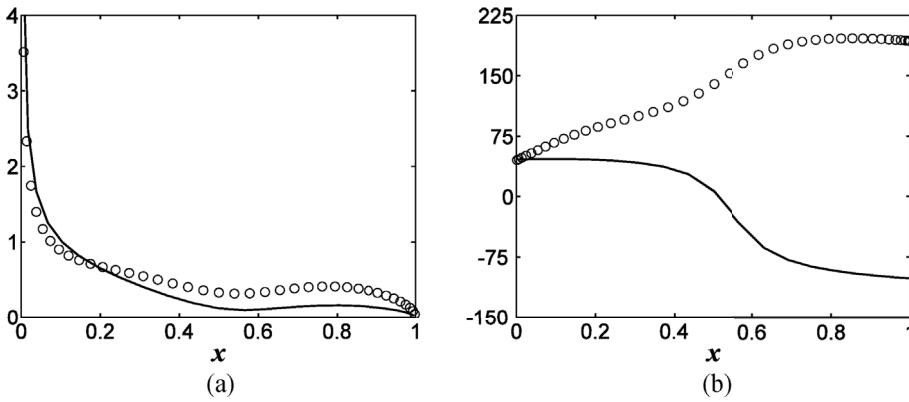
Fig. 10. Lift $\breve{L}(\xi)$ from gust - cascade interaction at a high frequency: (a) magnitude, (b) phase in degree. Vane count: 54, solidity: 1.7, $\theta = 10.29^0$, $\sigma = 0$, $M = 0.41$, $K_s = 11.56$, $\psi = 0^0$, $\alpha_s = 0^0$. 2-D equivalent parameters are the same as 3-D parameters. Solid line: 2-D equivalence + LINSUB, symbols: Adamczyk's high frequency approximation.

computation resources for high frequencies. When predicting broadband noise generated by fan wakes - OGV interactions in turbo-jet engines, analytical models such as Amiet's isolated-airfoil approximation are preferred. It is critical to identify the vane count limit (VCL), below which these analytical models are valid.

In an annular duct, sound power for the mth spinning mode and the nth radial mode is proportional to the chord-wise integrated lift at radius R [23]:

$$\widehat{h}_{mn}^{\pm}(k_1, k_2, k_3) = \left(\alpha_{mn}^{\pm} \sin\theta - \frac{m}{R}\cos\theta \right) \int\limits_{chord} e^{-i\xi\left(\alpha_{mn}^{\pm}\cos\theta + m\sin\theta/R\right)} \breve{L}(\xi, k_1, k_2, k_3) d\xi.$$

We study

$$\widehat{h}_s^{\pm} = \sqrt{\sum_{m,n} |\widehat{h}_{mn}^{\pm}|^2},$$
(41)

where the summation is carried out over all the cut-on modes in the duct. To evaluate VCL for realistic situations, we use the mean flow and the geometry from the NASA Source Diagnostic Test (SDT) at the approach condition [24]. Fig. 13 depicts a typical cascade response $\widehat{h}_s^+$ for sound waves in the downstream duct. It is compared with the response from the same gust interacting with isolated airfoils. It is noted that even at very low vane count, the cascade response is not the same as the isolated-airfoil response due to the IBPA effect discussed previously. However, the cascade effect is considered small if the difference of the two responses is less than 5%. For the case in Fig. 13, the cascade effect is small when the vane count is less than 20, *i.e.*, VCL = 20.
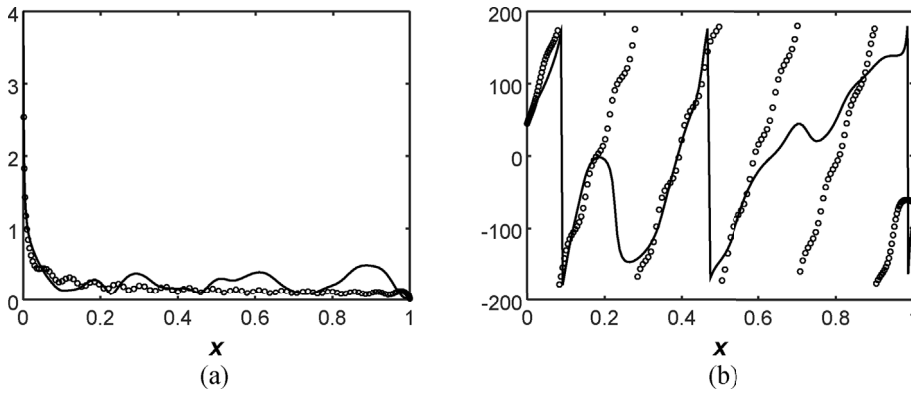
Fig. 11. Lift $\breve{L}(\xi)$ from gust - cascade interaction at a very high frequency: (a) magnitude, (b) phase in degree. Vane count: 30, solidity: 0.95, $\theta = 10.29^0$, $\sigma = 0$, $M = 0.41$, $K_s = 104$, $\psi = 0^0$, $\alpha_s = 0^0$. 2-D equivalent parameters are the same as 3-D parameters. Solid line: 2-D equivalence + LINSUB, symbols: Adamczyk's high frequency approximation.
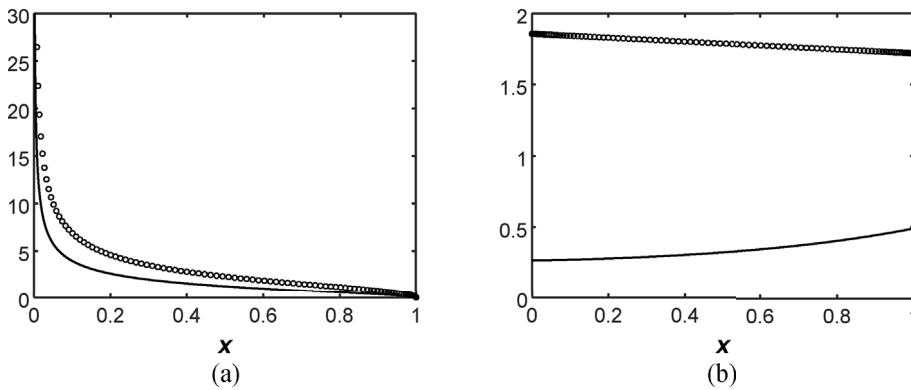
Fig. 12. Lift $\breve{L}(\xi)$ from gust - cascade interaction at low frequency: (a) magnitude, (b) phase in degree. Vane count: 54, solidity: 0.6, $\theta = 10.29^0$, $M = 0.5$, $\sigma = 0$, $K_s = 0.0072$, $\psi = 0^0$, $\alpha_s = 0^0$. 2-D equivalent parameters are the same as 3-D parameters. Solid line: 2-D equivalence + LINSUB, symbols: Adamczyk's low frequency approximation (Eq. (13) in Ref. [4]).
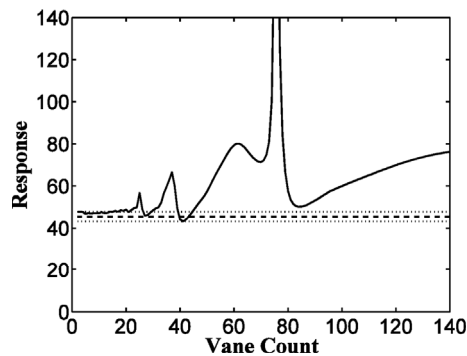
Fig. 13. Chord-wise integrated lift $\widehat{h}_s^+$ from gust − cascade interactions (solid line) and gust − isolated-airfoil interactions (dashed line). ±5% over the single-airfoil response are indicated by dotted lines.

A six-sigma statistics analysis was performed to find the key control parameters (KCP) for VCL. Four parameters were examined: sweep angle ψ in radians, Mach number M, reduced frequency λ, and spanwise wavenumber $k_3 \Lambda$. A matrix of 16 groups of parameters were chosen with $M = 0.4$ and 0.65, $\lambda = 2.24$ and 20.1, $k_3 \Lambda = 0$ and 0.12, $\psi = 0$ and 0.5236. The average VCL is found to be 14 with standard deviation of 3.3. A regression analysis was performed to obtain the transfer function from KCPs to VCL:

$$VCL \approx 7.06 + 17.7M - 68.7k_3\varLambda + 6.88\psi - 0.228\lambda. \tag{42}$$

Mach number is found to be the vital parameter among all the KCPs. VCL is higher at higher Mach number. Frequency is the least important. A general belief is that at high frequency, acoustic wavelength is small compared with the spacing between the airfoils; therefore the acoustic interaction is small. This study reveals the opposite trend, even though the frequency effect is small. The vane count of the baseline OGV in the SDT is 54, much larger than 14. Therefore, isolated-airfoil approximations are not applicable for SDT configurations.

8. Conclusions

The boundary value problem defined in terms of the acoustic velocity potential in the *Prandtl-Glauert* coordinate system has the same format for 2-D gusts and 3-D gusts. A 2-D equivalence method was developed accordingly to calculate the response from an oblique gust interacting with a linear cascade. Classic similarity rules for isolated airfoils and cascades were extended to account for spanwise mean flows. The formulas for the lift on the cascade and the acoustic pressure in the far-field were derived. In this method, only the inputs to a 2-D method need to be modified. It provides a convenient way to introduce oblique gusts and sweep into any 2-D models, such as the LINSUB [2] or the modified LINSUB [15]. Accuracy and effectiveness of this method combined with LINSUB were demonstrated.

The method was used to investigate the effect of gust angles. Two major effects are the spanwise phase variation and the lift magnitude factor $\overline{\beta}_M/\beta_M$ (ref. Eq. (34)). The 2-D equivalent lift doesn't vary much with the gust angle and can be approximated using a 2-D model.

Cascade effects due to IBPA and solidity were studied. Overall, a cascade has a stronger effect on lift phase than on its magnitude. IBPA effect is important even for very low solidity. As cascade solidity increases, lift becomes less leading-edge dominant. A statistical analysis was carried out to evaluate the vane count limit for small cascade effects. The transfer function from KCPs to VCL was established. It was found that Mach number is the vital parameter. The sweep angle and the span-wise wavenumber are less important. Frequency is least important among all KCPs.

This method was employed in the investigation of fan wakes − OGV interaction broadband noise and was validated against the NASA SDT data in Ref. [23].

Appendix A. Supplementary data

Supplementary data related to this article can be found at https://doi.org/10.1016/j.jsv.2018.08.013.

Appendix. Proof of Eq. (38)

Substituting the coordinate transformation Eq. (8) into Eq. (35), we obtain Eq. (36) for the acoustic wave in the duct coordinate system with

$$\beta_r = \overline{\beta}_r \sin\theta/\sin\overline{\theta} + \left(1 - \overline{\beta}_M^2\Big/\beta_M^2\right)\omega_e \sin\theta\Big/u_{0\xi}, \tag{A1}$$

$$\alpha_r^{\pm} = \overline{\alpha}_r^{\pm} \cos\overline{\theta}\Big/\cos\theta + \overline{\beta}_r \sin\theta \cos\overline{\theta}\left(\overline{\beta}_M\Big/\beta_M - \beta_M\Big/\overline{\beta}_M\right) + \left(1 - \overline{\beta}_M^2\Big/\beta_M^2\right)k_{s1} \cos\theta. \tag{A2}$$

From Eqs. (35) and (32),

$$\overline{\beta}_r = \overline{\beta}_s - 2\pi r\Big/\overline{S} = \left\{\beta_s + \sin\theta\left[\left(\overline{\beta}_M\Big/\beta_M\right)^2 - 1\right]\lambda_e - 2\pi r/S\right\}\Big/\left[\sin^2\theta + \cos^2\theta\left(\beta_M\Big/\overline{\beta}_M\right)^2\right]^{1/2}.$$

Substituting it into Eq. (A1), one has

$$\beta_r = \beta_s - 2\pi r/S.$$

From Eqs. (A1), (35), and (32),

$$\alpha_r^{\pm} = \frac{u_{0x}\left(-\omega + \beta_r u_{0y} + k_3 u_{0z}\right)\cos^2\overline{\theta}\,\overline{\beta}_M^2 \Big/ \left(\beta_M^2 \cos\theta\right) \pm \cos\overline{\theta}\sqrt{\left(\overline{\omega} - \overline{\beta}_r \overline{u}_{0y}\right)^2 - \overline{\beta}_r^2\left(1 - \overline{u}_{0x}^2\right)}}{\cos\theta\left(1 - \overline{u}_{0x}^2\right)}.$$

Since

$$\left(\overline{\omega} - \overline{\beta}_r \overline{u}_{0y}\right)^2 - \overline{\beta}_r^2\left(1 - \overline{u}_{0x}^2\right)$$

$$= \left(\overline{\beta}_M/\beta_M\right)^4\left(\cos^2\overline{\theta}\big/\cos^2\theta\right)\Big[\left(u_{0\xi}k_{s1} - \beta_r u_{0y}\right)^2 - \left(\beta_r^2 + k_3^2\right)\left(1 - u_{0x}^2\right)$$

$$+ k_{s1}^2 \overline{u}_{0\xi}^2\left(\cos^2\theta - \cos^2\overline{\theta} - u_{0\xi}^2\cos^2\theta\sin^2\overline{\theta} + \overline{u}_{0\xi}^2\sin^2\theta\cos^2\overline{\theta}\right)\big/\left(\beta_M^2\cos^2\overline{\theta}\right)\Big]$$

$$= \left(\overline{\beta}_M/\beta_M\right)^4\left(\cos^2\overline{\theta}\big/\cos^2\theta\right)\Big[\left(u_{0\xi}k_{s1} - \beta_r u_{0y}\right)^2 - \left(\beta_r^2 + k_3^2\right)\left(1 - u_{0x}^2\right)\Big],$$

then

$$\alpha_r^{\pm} = \frac{\cos^2\overline{\theta}\,\overline{\beta}_M^2\big/\left(\beta_M^2\cos\theta\right)}{\cos\theta\left(1 - \overline{u}_{0x}^2\right)}\Big[u_{0x}\left(-\omega + \beta_r u_{0y} + k_3 u_{0z}\right) \pm \sqrt{\left(u_{0\xi}k_{s1} - \beta_r u_{0y}\right)^2 - \left(\beta_r^2 + k_3^2\right)\left(1 - u_{0x}^2\right)}\Big]$$

$$= \frac{u_{0x}\left(-\omega + \beta_r u_{0y} + k_3 u_{0z}\right) \pm \sqrt{\left(\omega - \beta_r u_{0y} - k_3 u_{0z}\right)^2 - \left(\beta_r^2 + k_3^2\right)\left(1 - u_{0x}^2\right)}}{1 - u_{0x}^2}.$$

References

[1] B.L. Morin, Broadband Fan Noise Prediction System for Turbofan Engines, vol. 1, Setup_BFaNS User's Manual and Developer's Guide, November 2010. NASA/CR-2010-216898.
[2] S.N. Smith, Discrete Frequency Sound Generation in Axial Flow Turbomachines, 1973. ARC R. & M. No. 3709.
[3] J.J. Adamczyk, R.S. Brand, Scattering of sound by an aerofoil of finite span in a compressible stream, J. Sound Vib. 25 (1972) 139–156.
[4] J.J. Adamczyk, Passage of a swept airfoil through an oblique gust, J. Aircraft 11 (5) (1974).
[5] R.K. Amiet, High frequency thin-airfoil theory for subsonic flow, AIAA J. 14 (8) (1976) 1076–1082.
[6] M. Roger, C. Schramb, S. Moreau, On vortex–airfoil interaction noise including span-end effects, with application to open-rotor aeroacoustics, J. Sound Vib. 333 (2014) 283–306.
[7] S.A.L. Glegg, The response of a swept blade row to a three-dimensional gust, J. Sound Vib. 227 (1) (1999) 29–64.
[8] H. Posson, M. Roger, S. Moreau, On a uniformly valid analytical rectilinear cascade response function, J. Fluid Mech. 663 (2010) 22–52.
[9] E. Envia, in: A High Frequency Model of Cascade Noise, AIAA Paper 1998-2318, 4th AIAA/CEAS Aeroacoustics Conference, Toulouse, France, June 1998.
[10] M. Namba, Three-dimensional analysis of blade force and sound generation for an annular cascade in distorted flows, J. Sound Vib. 50 (4) (1977) 479–508.
[11] C.S. Ventres, M.A. Theobald, W.D. Mark, Turbofan Noise Generation, vol. 1, 1982. Analysis, NASA CR-167952.
[12] D.B. Hanson, Theory for Broadband Noise of Rotor and Stator Cascades with Inhomogeneous Inflow Turbulence Including Effects of Lean and Sweep, NASA CR-2001-210762.
[13] M. Nallasamy, E. Envia, Computation of rotor wake turbulence noise, J. Sound Vib. 282 (2005) 649–678.
[14] C. Cheong, P. Joseph, S. Lee, High frequency formulation for the acoustic power spectrum due to cascade-turbulence interaction, J. Acoust. Soc. Am. 119 (1) (2006).
[15] R.A. Reba, B.L. Morin, The gust response of an acoustically treated flat-plate cascade, in: AIAA paper 2008-2898, 14th AIAA/CEAS Aeroacoustics Conference, Vancouver, Canada, May 2008.
[16] S.M. Grace, A. Wixom, J. Winkler, D.L. Sondak, M.M. Logue, Fan broadband interaction noise modeling, in: AIAA paper 2012-2269, 18th AIAA/CEAS Aeroacoustics Conference, Colorado Springs, June 2012.
[17] M.E. Goldstein, Aeroacoustics, NASA SP-346, 1976.
[18] L.T. Filotas, Theory of Airfoil Response in a Gusty Atmosphere, Part I - Aerodynamic Transfer Function. UTIAS-139, Toronto University, 1969.
[19] B.D. Mugridge, Gust loading on a thin, Airfoil. Aeron. Quart. 22 (3) (Aug. 1971) 301–310.
[20] R. Martinez, S.E. Widnall, Unified aerodynamic-acoustic theory for a thin rectangular wing encountering a gust, AIAA J. 18 (1980) 636–645.
[21] H. Atassi, G. Hamad, Sound generated in a cascade by the three-dimensional disturbances convected in subsonic flow, in: AIAA Paper 1981-2046, 7th AIAA Aeroacoustics Conference, Palo Alto, California, 1981.
[22] A.E.D. Lloyd, N. Peake, Rotor-stator broadband noise prediction, in: AIAA paper 2008-2840, 14th AIAA/CEAS Aeroacoustics Conference (29th AIAA Aeroacoustics Conference), Vancouver, Canada, May 2008.
[23] H. Ju, R. Mani, M. Vysohlid, A. Sharma, Investigation of fan wake - OGV interaction broadband noise, AIAA J. 53 (12) (2015) 3534–3550.
[24] C.E. Hughes, Aerodynamic performance of scale-model turbofan outlet guide vanes designed for low noise, in: AIAA paper 2002-0374, 40th AIAA Aerospace Sciences Meeting & Exhibit, Reno,NV,U.S.A, Jan, 2002.
[25] S.M. Grace, Fan broadband interaction noise modeling using a low-order method, J. Sound Vib. 346 (1) (2015) 402–423.
[26] H. Posson, S. Moreau, Effect of rotor shielding on fan-outlet guide vanes broadband noise prediction, AIAA J. 51 (7) (2013) 1576–1592.
[27] J.R. Gill, X. Zhang, P. Joseph, T. Node-Langlois, Reduced dimension modeling of leading edge turbulent interaction noise, in: AIAA paper 2014-2321, 20th AIAA/CEAS Aeroacoustics Conference, Atlanta, June 2014.
[28] J.M.R. Graham, Similarity rules for thin aerofoils in non-stationary subsonic flows, J. Fluid Mech. 43 (4) (1970) 753–766.